ISSN: 2688-8645

Mass Transfer in CO_2 Huff-Puff of Shale Oil Reservoirs

Zijiang Yang, Haikun Zeng

School of Petroleum Engineering, Xi'an Shiyou University, Xi'an Shaanxi, 710065, China

Abstract

Experimental study on the influencing factors of CO_2 injection to enhance oil recovery in shale oil reservoirs using nuclear magnetic resonance (NMR) technology. The effects of action time, pressure, and temperature on enhanced oil recovery were analyzed based on the NMR T_2 (transverse relaxation time) spectrum, and the oil displacement effect of CO_2 on crude oil was observed through NMR images. Then, molecular dynamics simulation methods were used to study the interaction laws and mass transfer characteristics between crude oil and carbon dioxide under different conditions, and the results of macroscopic experiments were analyzed using the insights obtained from microscopic simulations. The study shows that during the CO_2 injection process, the recovery degree gradually increases with the extension of the action time. As the pressure increases, the recovery degree gradually rises. With the increase in temperature, the recovery degree of shale oil first increases and then gradually decreases. Under immiscible conditions, the recovery degree of crude oil in macropores increases rapidly with the increase of injection pressure; under miscible conditions, the impact of increased injection pressure on the recovery degree of macropores weakens. Regardless of miscibility, the recovery degree of crude oil in micropores basically shows a linear growth with the increase of injection pressure, and as the gas injection pressure increases, the lower limit of CO_2-accessible pore size continues to decrease. With the increase of soaking time, the growth rate of crude oil recovery degree in macropores gradually decreases, while the growth rate of crude oil recovery degree in micropores first increases and then decreases.

Keywords

Shale Oil; CO_2 huff-n-puff; NMR; Molecular Simulation.

1. Introduction

After the shale gas revolution, shale oil has become a new direction and hotspot in the global exploration and development of unconventional oil and gas, with commercial development already carried out worldwide. China is rich in shale oil resources, and the estimated geological resource volume of medium-to-high maturity shale oil is approximately 13.2×10^8 tons, making it the most important substitute resource for future oil exploration and development in China [1]. However, shale oil reservoirs are characterized by underdeveloped natural fractures, widespread nanoscale pores, extremely low porosity and permeability, and complex pore-throat structures, making it difficult to obtain effective productivity through conventional development methods. It is usually necessary to rely on large-scale volume fracturing and other means to transform shale tight reservoirs, and then improve the flow properties of shale oil by injecting gas, so as to increase its recovery rate.

Carbon dioxide is colorless, odorless, stable in properties, non-flammable, easy to liquefy and recycle under normal temperature and pressure. When the temperature reaches 30.98°C and the pressure exceeds 7.38MPa, carbon dioxide is in a supercritical state, with both the density of liquid and the viscosity of gas, as well as a high diffusion coefficient, strong penetration ability and good heat and mass transfer performance [2]. For shale reservoirs with strong water

ISSN: 2688-8645

sensitivity, injecting carbon dioxide can effectively avoid the expansion of shale clay caused by water flooding for oil recovery. In addition, due to the strong adsorption characteristics of carbon dioxide, alkane molecules such as methane in shale can be displaced by the injected carbon dioxide, which increases the yield of light hydrocarbons and realizes the storage of carbon dioxide. Therefore, carbon dioxide is usually the main choice of injection gas for improving oil recovery.

CO_2 capture, utilization, and storage (CCUS) is an important emission reduction technology for addressing climate change, achieving the goals of the Paris Agreement, and realizing carbon neutrality in the future [3]. Combining CO_2 geological storage with enhanced oil recovery (CO_2-EOR) can meet the dual needs of carbon emission reduction and energy development, showing broad application prospects [4]. The development of oil and gas in tight sandstone reservoirs is an important part of unconventional energy development [5]. Countries such as the United States and Canada have successfully carried out large-scale industrial exploitation, and China has also carried out extensive large-scale development in basins such as Ordos, Junggar, and Sichuan [6]. Compared with waterflood development, injecting CO_2 into tight sandstone reservoirs can more effectively exploit crude oil, improve the flow capacity of reservoir fluids, and timely supplement formation energy. In view of the current development trend of carbon neutrality and the industrial application foundation of CO_2-EOR, CO_2-EOR projects in tight sandstone reservoirs will further increase in the future. Therefore, it is very necessary to study the interaction mechanism between CO_2 and tight sandstone reservoir fluids in pore media. However, in tight sandstone reservoirs, due to the development of nanoscale pore throats, the interface effects between fluids and between fluids and pore walls are very obvious, and the intermolecular forces cannot be ignored. Conventional experimental methods are difficult to reveal the essence of experimental phenomena. Molecular dynamics simulation can make up for the shortcomings of traditional experiments and numerical methods. After decades of development, it can characterize the interactions between different fluids and between fluids and pore walls in pore media from the molecular scale, and can quantitatively describe the energy and dynamic structural characteristics of fluids in the system [7].

2. Study on CO_2 Diffusion and Mass Transfer Mechanism in Multi-Scale Media

2.1. Nuclear Magnetic Resonance (NMR) Experiment on CO_2 Huff and Puff in Shale Oil of the Study Area

2.1.1. NMR Experiment of CO_2 Huff and Puff in Shale Oil

Using MRI nuclear magnetic resonance imaging device and core flooding device, the data of PVT tight sand-packed tubes under different temperature and pressure conditions were tested in terms of miscibility pressure, concentration diffusion range, miscibility area, etc. In the MRI nuclear magnetic resonance imaging system, the oil phase generates 1H signals, while CO_2 generates no signals. Therefore, the T_2 inversion spectrum can be used to observe the utilization of core pores, and the change of imaging maps can be used to characterize the mass transfer and diffusion process of the CO_2-shale oil system[8-10].

Experimental Equipment: Reciprocating Pump; Constant Temperature System; Thermocouple Temperature Control System; Pressure Acquisition System; Nuclear Magnetic Resonance Imaging (NMRI) System.

Experimental Materials: Crude oil produced from typical blocks in Area X;CO_2(purity > 99.9%);Rock samples from well sites in typical areas of Area X.

ISSN: 2688-8645

Table 1. Summary of Core Data

Core Number	Diameter(cm)	Length(cm)	Porosity(%)	Permeability/10-^{3}μm^{2}
Y48-1-2	2.48	6.430	7.4	0.070
B75-2-2	2.49	6.510	7.2	0.068
Y48-2-2	2.48	6.450	7.1	0.071
Z16-3	2.49	6.530	7.0	0.072
LI434-2	2.49	6.310	7.1	0.081

Experimental Method:

1) Core Saturation and Pre-Experiment Scanning

Connect the experimental pipeline system and saturate the core with crude oil using a reciprocating pump at a flow rate of 0.15 ml/min for 24 hours under a constant confining pressure of 20 MPa.

After aging and drying the core, obtain T2 inversion spectra and MRI images using a nuclear magnetic resonance (NMR) system to characterize the initial pore structure.

2) CO_2 Injection and Soaking Process

Adjust the temperature control system to the target temperature and stabilize.

Set the confining pressure to 1–2 MPa higher than the CO2 injection pressure (e.g., if injection pressure = 15 MPa, confining pressure = 16–17 MPa).

Initiate CO2 injection at a rate of 0.25 ml/min under constant pressure. Stop injection when the cumulative CO2 volume reaches 1.2 PV (pore volumes).

After injection, close all valves and initiate the soaking period (duration specified by experimental design).

3) Pressure Relief and Post-Experiment Analysis

After the soaking period, gradually reduce pressure to atmospheric level in stages.

Record pressure, oil production volume, and time-series data until oil production ceases.

Perform post-soaking T2 spectral analysis and MRI imaging to characterize changes in pore fluid distribution and analyze CO2-oil mass transfer mechanisms within micro-nanopores.

Table 2. Experimental Schemes

Scheme No.	Reservoir Temperature(℃)	Injection Pressure(MPa)	Soaking Time(h)
1	40	10	1,4,8
2		15	1,4,8
3		20	1,4,8
4	60	10	1,4,8
5		15	1,4,8
6		20	1,4,8
7	80	10	1,4,8
8		15	1,4,8
9		20	1,4,8

2.1.2. Experimental Results and Analysis

NMR Images Before and After the Experiment under Conditions of 313K and 10MPa:

ISSN: 2688-8645

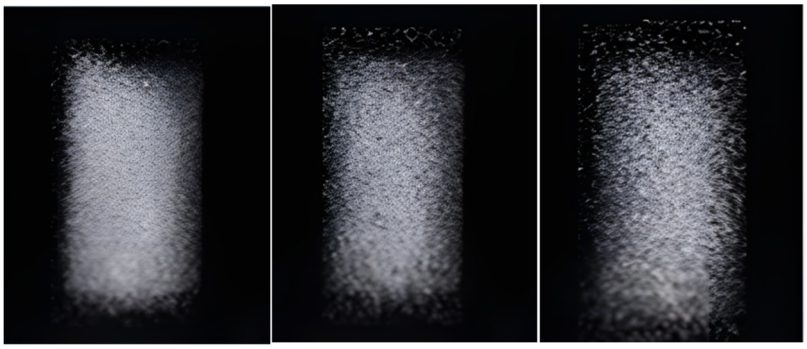

(a) Interaction Time:1 hour(b) Interaction Time: 4 hours(c) Interaction Time: 8 hours

Figure 1. NMR Images of Core Y48-1-2 with Different CO_2 Interaction Times

NMR Images Before and After the Experiment under Conditions of 313K and 15MPa:

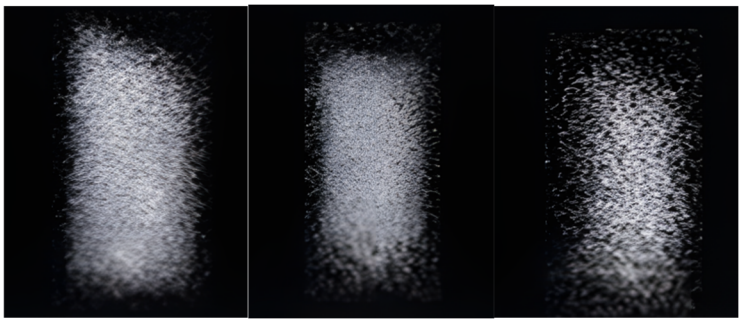

(a) Interaction Time:1 hour(b) Interaction Time: 4 hours(c) Interaction Time: 8 hours

Figure 2. NMR Images of Core Y48-1-2 with Different CO_2 Interaction Times

NMR Images Before and After the Experiment under Conditions of 313K and 20MPa:

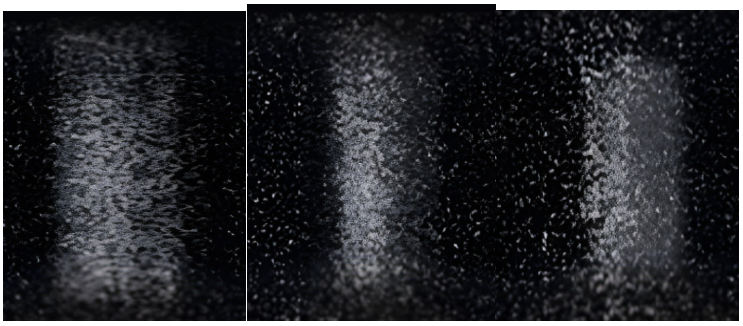

(a) Interaction Time:1 hour(b) Interaction Time: 4 hours(c) Interaction Time: 8 hours

Figure 3. NMR Images of Core Y48-1-2 with Different CO_2 Interaction Times

NMR Images Before and After the Experiment under Conditions of 333K and 10MPa:

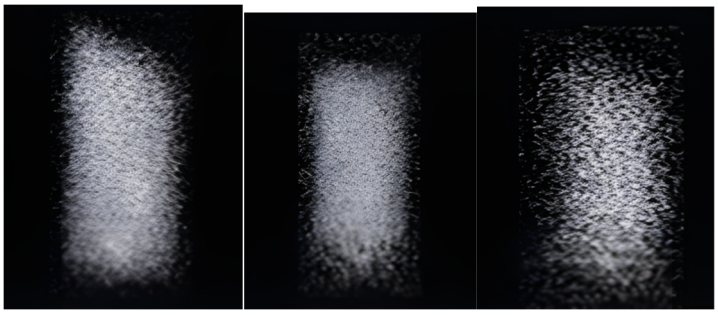

(a) Interaction Time:1 hour(b) Interaction Time: 4 hours(c) Interaction Time: 8 hours

Figure 4. NMR Images of Core Y48-2-2 with Different CO_2 Interaction Times

ISSN: 2688-8645

NMR Images Before and After the Experiment under Conditions of 333K and 15MPa:

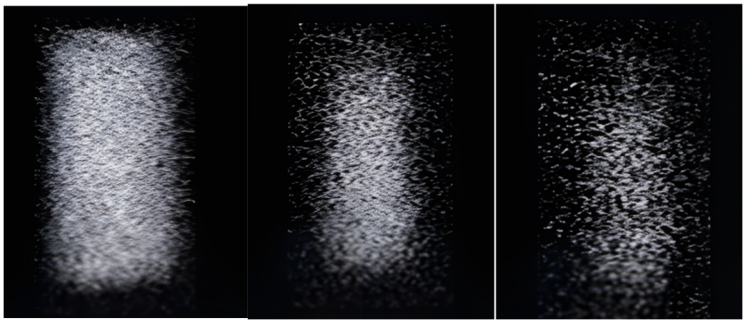

(a) Interaction Time:1 hour(b) Interaction Time: 4 hours(c) Interaction Time: 8 hours

Figure 5. NMR Images of Core Y48-2-2 with Different CO_2 Interaction Times

NMR Images Before and After the Experiment under Conditions of 333K and 20MPa:

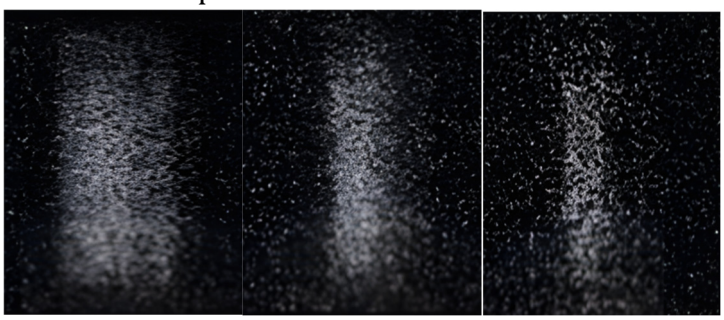

(a) Interaction Time:1 hour(b) Interaction Time: 4 hours(c) Interaction Time: 8 hours

Figure 6. NMR Images of Core Y48-2-2 with Different CO_2 Interaction Times

NMR Images Before and After the Experiment under Conditions of 353K and 10MPa:

(a) Interaction Time:1 hour(b) Interaction Time: 4 hours(c) Interaction Time: 8 hours

Figure 7. NMR Images of Core Z16 with Different CO_2 Interaction Times

NMR Images Before and After the Experiment under Conditions of 353K and 15MPa:

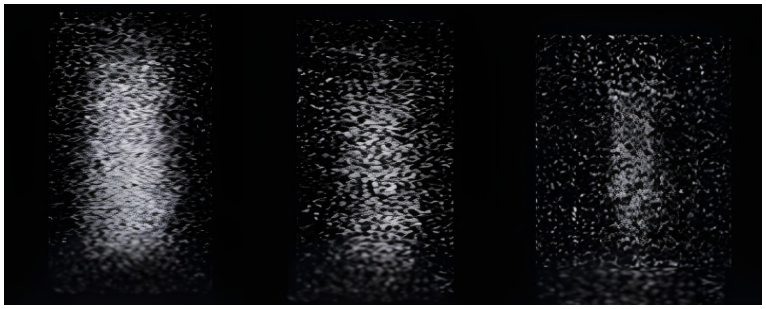

(a) Interaction Time:1 hour(b) Interaction Time: 4 hours(c) Interaction Time: 8 hours

Figure 8. NMR Images of Core Z16 with Different CO_2 Interaction Times

ISSN: 2688-8645

NMR Images Before and After the Experiment under Conditions of 353K and 20MPa:

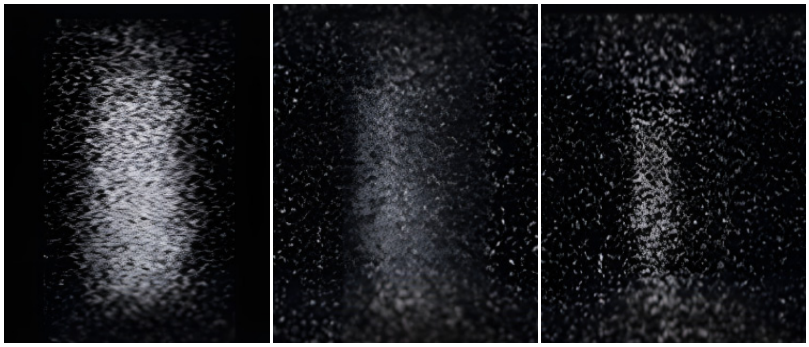

(a) Interaction Time:1 hour(b) Interaction Time: 4 hours(c) Interaction Time: 8 hours

Figure 9. NMR Images of Core Z16 with Different CO_2 Interaction Times

2.1.3. Experimental Data Processing and Diffusion Coefficient Determination

Assumptions of the Diffusion Mathematical Model:

In this experiment, the pressure decay method is used to calculate the diffusion coefficient of the CO_2-crude oil system in porous media. The pressure decay method is based on Fick's diffusion equation, establishing a mathematical model that describes the diffusion process of CO_2 in crude oil-saturated porous media according to the physical model of the diffusion experiment. First, the following assumptions are made:

(1) The change in system concentration during the experiment has no significant effect on the diffusion coefficient, i.e., the diffusion coefficient remains constant during the diffusion process.

(2) The mass transfer resistance at the gas-liquid interface can be ignored, meaning that equilibrium boundary conditions are applied to the gas-liquid contact interface in porous media. The concentration of each component at the interface is always considered to be the equilibrium concentration.

(3) The system temperature remains constant throughout the experiment, and there is no molecular movement of gas-liquid phases at the end of the porous media. Specifically, the terminal has no gas components, and the CO_2 concentration is always zero.

(4) During the diffusion experiment, the swelling effect of liquid crude oil and natural convection caused by density differences are ignored, with only molecular diffusion considered.

(5) The injected gas phase maintains a single component to avoid the influence of multi-components. In this experiment, the one-dimensional axial diffusion system is placed horizontally to eliminate the influence of gravity on diffusion results and reduce non-molecular diffusion (convective diffusion) during the process. The physical model is shown in Figure 10[11-13].

(6)

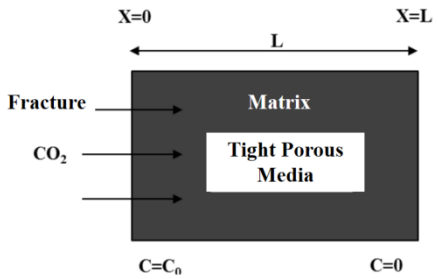

Figure 10. Physical Model of Diffusion in Porous Media

Based on Fick's theorem mentioned above, the diffusion coefficient is derived from the law of mass conservation and the real gas equation of state by calculating the pressure drop.

ISSN: 2688-8645

According to the pressure decline data from the diffusion experiment, $\Delta P = P(t) - P_0$ between $\Delta\sqrt{t} = \sqrt{t} - \sqrt{t_0}$ is plotted. By fitting the linear segment to obtain the coefficient a in the correlation equation, the effective diffusion coefficient D_e for this group of experiments can be calculated using Equation (1):

$$D_e = \left(\frac{aV_g\tau\sqrt{\pi}}{2C_0Z_gRTA_s\emptyset}\right)^2 \quad (1)$$

Taking the experiment of determining the effective diffusion coefficient of the CO_2-crude oil system in porous media under an initial injection pressure within the range of 10 MPa at an experimental temperature of 40°C as an example, the following is the data curve plotted from the results.

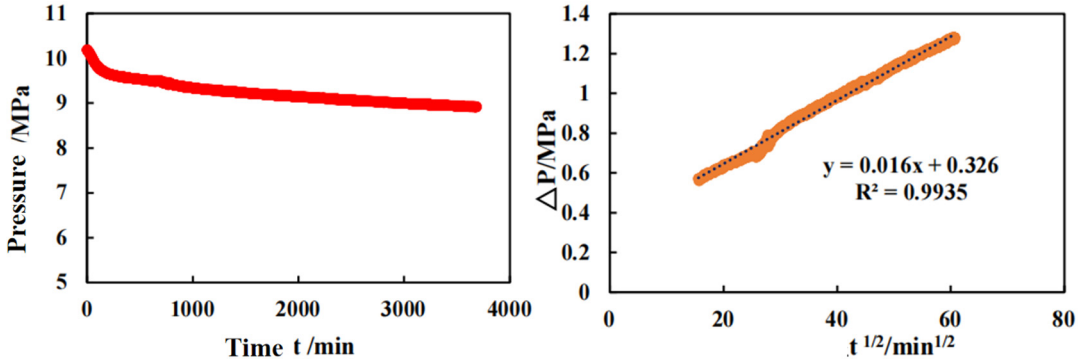

(a) Pressure Drop Curve (b) Pressure Difference Curve

Figure 11. Diffusion Results of CO_2-Crude Oil System in Porous Media at 10 MPa

Table 3. Calculation Results of Diffusion Coefficients

Temperature/°C	Pressure/MPa		Permeability/$10^{-3}\mu m^2$	Porosity/%	Tortuosity	Initial Concentration/(mol/L)	Slope/a	Diffusion Coefficient($10^{-8}m^2/s$)
	Initial Pressure	Equilibrium Pressure						
40	10.1	8.91	0.070	7.4	5.89	13.72	0.016	1.193
40	15	9.33	0.071	7.2	5.24	16.45	0.0571	1.372
40	20.8	12.64	0.072	7.1	5.04	20.23	0.1015	1.453
60	10	7.68	0.068	7.0	4.89	12.52	0.1049	2.003
60	15	11.8	0.081	7.1	5.04	16.29	0.1018	2.262
60	20.2	13.07	0.070	7.4	5.89	22.23	0.0754	2.403
80	10	9.08	0.071	7.2	5.24	13.72	0.2996	2.203
80	15	12.27	0.072	7.1	5.04	15.46	0.4598	2.472
80	20	10.88	0.72	7.1	5.04	20.23	0.0624	2.603

ISSN: 2688-8645

A total of 9 groups of results were calculated by Formula (1) under different temperature and pressure conditions, as shown in Table 3.

Analysis shows that during CO_2 injection, carbon dioxide exerts twofold effects on crude oil in the core: Under external pressure, the two-phase interface formed by CO_2 and crude oil pushes oil in macropores to migrate toward fractures or regions with low capillary resistance (in this experiment, due to the NMR device's limitations, a segment near the sealed end remained unfilled by fluid, which can be equivalent to a fracture region with low seepage resistance).CO_2 drives oil into medium and small pores, increasing oil content in these pores. Under the balance of external force and capillary resistance, convective mass transfer occurs between CO_2 and oil phases. CO_2 dissolves and mixes with oil through molecular diffusion and convective mass transfer, altering oil properties—some light hydrocarbons are extracted during CO_2 movement. The diffusion phenomenon becomes more pronounced with increasing temperature and pressure.

2.2. Study on Microscopic Mechanism of CO_2 Injection-induced Diffusion Mass Transfer

2.2.1. Model Establishment

Octane was selected as the main crude oil component. Energy and geometry optimization were performed on heptane molecules and other molecules to obtain their minimum energy configurations. CO_2 molecules in the minimum energy configuration were constructed using the same method. The Construction task in the Amorphous Cell module was used to build a crude oil box with a density of 0.7g/cm^3, containing 303 heptane molecules. The size of the crude oil box was 30 Å × 30 Å × 80 Å.

Table 4. Compositional Analysis Data of Formation Fluid Wellstream

Component	Flash Oil Composition(mol%)	Flash Gas Composition(mol%)	Wellstream Composition(mol%)
N_2	0	1.199	0.672
CO_2	0	0.573	0.322
C_1	0.411	53.498	30.194
C_2	0.536	16.714	9.612
C_3	1.75	14.351	8.819
iC_4	0.411	2.139	1.381
nC_4	3.588	5.524	4.674
iC_5	2.173	1.767	1.946
nC_5	3.179	1.75	2.377
C_6	5.151	1.567	3.14
C_7	5.177	0.743	2.689
C_8	15.971	0.174	7.109
C_9	5.585	0	2.452
C_{10}	3.607	0	1.583
C_{11+}	52.462	0	23.03
Total	100	100	100

ISSN: 2688-8645

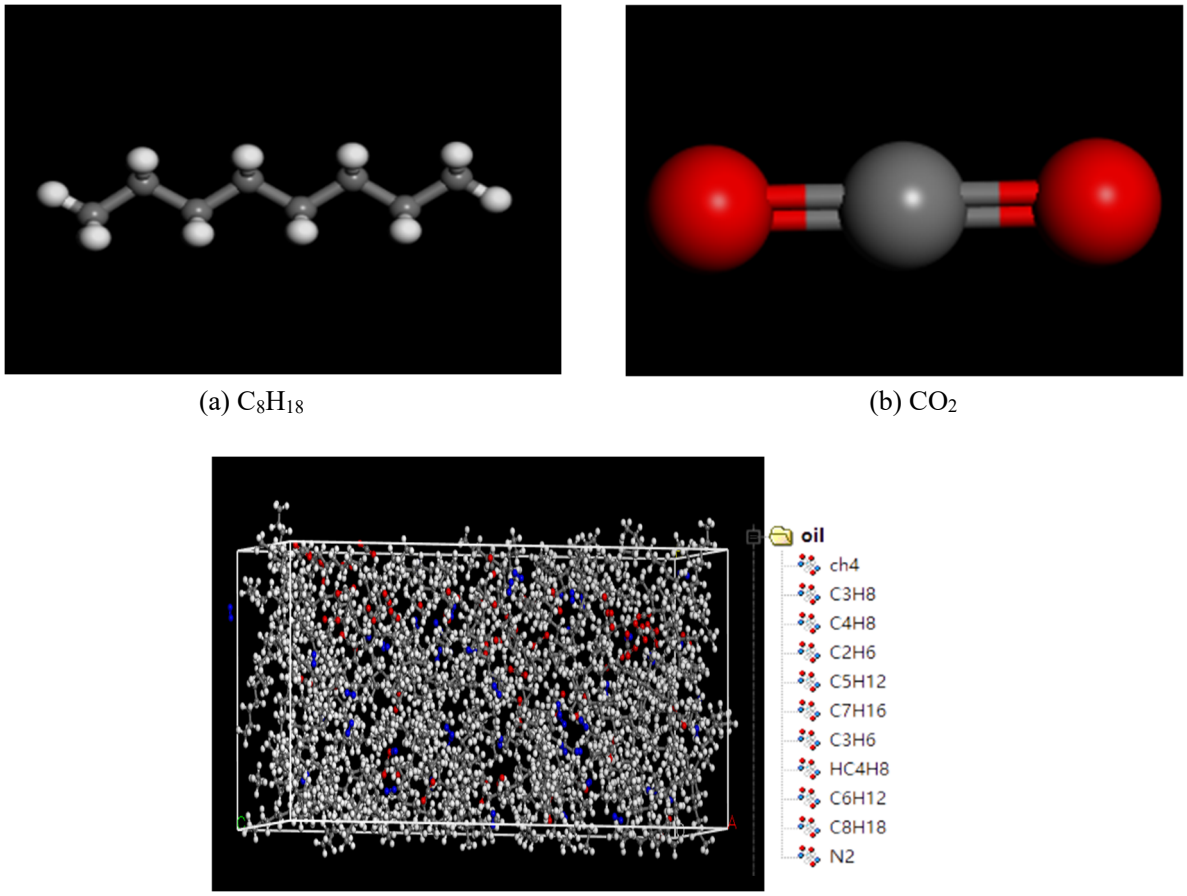

(a) C_8H_{18} (b) CO_2

Figure 12. Optimized Molecular Configurations and Model Diagrams of Octane and Carbon Dioxide

2.2.2. Simulation Condition Settings

Based on the known production data, the Hua H17 Platform has an average burial depth of 2039 m, with an initial formation pressure of 16.0 MPa and a formation temperature of 67.3°C. Therefore, the designed maximum temperature is 80°C and the minimum is 40°C. The minimum miscible pressure measured by previous capillary tube experiments is 14.35 MPa, so the pressures are designed as 10 MPa, 15 MPa, and 20 MPa. Models were designed under different pressure and temperature conditions.

2.2.3. Simulation Results and Analysis

Through Monte Carlo simulations of CO_2 molecular dissolution and diffusion in crude oil system models under different conditions, as well as NPT and NVT molecular dynamics simulations of the crude oil model before and after CO_2 dissolution, the volume strain and viscosity changes in the crude oil system induced by temperature and pressure variations were obtained. This allows for a comparative investigation of the effects of temperature, pressure, and CO_2 dissolution on crude oil volume expansion and viscosity reduction, and the calculation of diffusion coefficients[14-15].

Mean Square Displacement (MSD) and Diffusion Coefficient (D):

$$MSD(t) = \langle |\bar{r}(t) - \bar{r}(0)|^2 \rangle = \frac{1}{N}\sum_{i=1}^{N} |\bar{r}(t) - \bar{r}(0)|^2$$

The diffusion coefficient D is one-sixth of the slope of the MSD curve. After performing two NVT molecular dynamics simulations, MSD data are respectively obtained, and the bulk diffusion coefficients under different conditions are calculated through the mean square displacement. Taking 313 K and 20 MPa as an example.

ISSN: 2688-8645

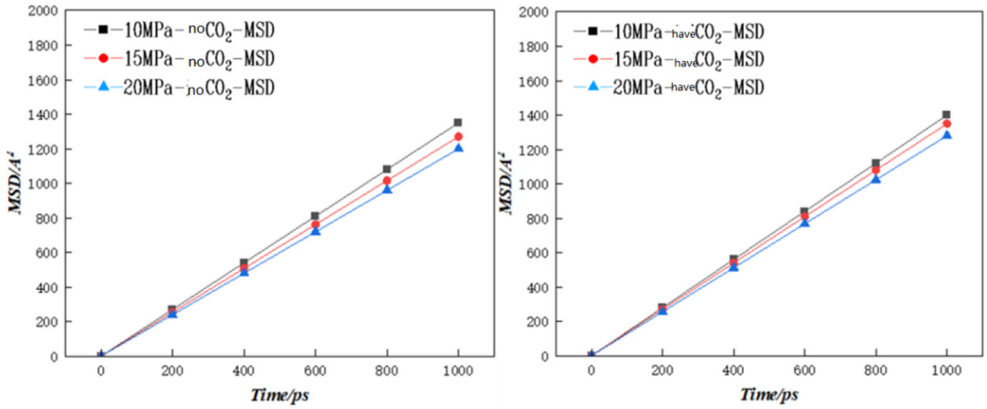

(a).System without CO_2 (b). System with CO_2

Figure 13. MSD Curves of Crude Oil Molecules as a Function of Simulation Time under Different Conditions (313 K, 10 MPa)

Through NVT molecular dynamics simulations, the motion of molecules under equilibrium conditions at corresponding pressures and temperatures can be obtained. The figure shows the mean square displacement (MSD) versus simulation time curves for the crude oil system before and after CO_2 dissolution under different pressures and temperatures. Based on the formula, the diffusion coefficient Dis one-sixth of the slope of the MSD-time curve. By calculating the slopes of the curves in the figure, diffusion coefficients of crude oil molecules under various temperature and pressure conditions are obtained.

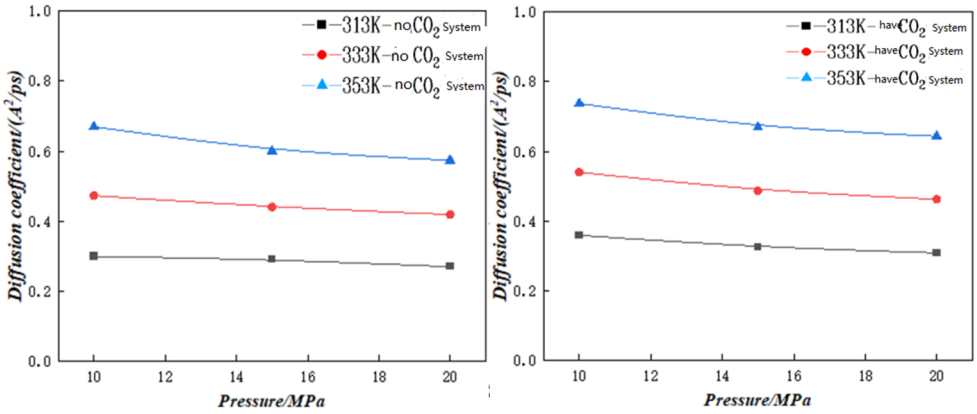

(a).System without CO_2 (b). System with CO_2

Figure 14. Diffusion Coefficients of Crude Oil System Before and After CO_2 Dissolution as a Function of Temperature and Pressure

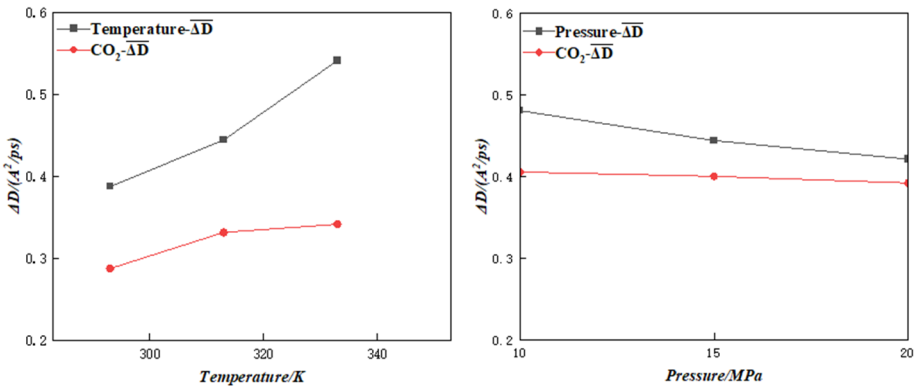

Figure 15. Curves of Average Diffusion Coefficient vs. Temperature and Pressure under Different Conditions

ISSN: 2688-8645

The figure displays curves of diffusion coefficients for the crude oil system before and after CO_2 dissolution as functions of temperature and pressure. As shown, with increasing pressure, the crude oil model is compressed, leading to an increase in fluid viscosity. Consequently, the diffusion coefficients of both the CO_2-dissolved and pure crude oil systems decrease, indicating weakened molecular diffusion capability. When temperature rises, molecular thermal motion intensifies, causing the diffusion coefficient to exhibit an upward trend with increasing temperature. After CO_2 dissolution, the presence of CO_2 in the intermolecular spaces of crude oil reduces intermolecular forces and frictional resistance during molecular motion, thereby enhancing the diffusion coefficient.

To compare the effects of temperature, pressure, and CO_2 dissolution on the diffusion coefficient of crude oil systems, average diffusion coefficients under various factor systems were calculated, and their relationship curves were obtained. The results show that increasing temperature significantly promotes the diffusion of crude oil molecules, while the promoting effect of dissolved CO_2 remains at a low and stable level.

With the increase in pressure, the average diffusion coefficient of crude oil molecules decreases, but the magnitude is small, within the range of approximately 0.05×10^{-7} cm^2/s. This is because the increase in pressure promotes more CO_2 to enter the intermolecular spaces of crude oil, which helps reduce the intermolecular interactions to a certain extent.

2.3. Molecular Simulation of Carbon Dioxide and Crude Oil in Porous Media

2.3.1. Foundation Model Establishment

First, using Material Studio software, the energy and geometry optimized heptane molecules, carbon dioxide molecules, and argon atoms were constructed into corresponding initial boxes. As shown in the figure, there are 303 heptane molecules in a box with the size of 30Å×30Å×80Å; the carbon dioxide box has a size of 30Å×30Å×50Å with 493 carbon dioxide molecules; and the argon plate box has a size of 30Å×30Å×2Å with 225 argon atoms.

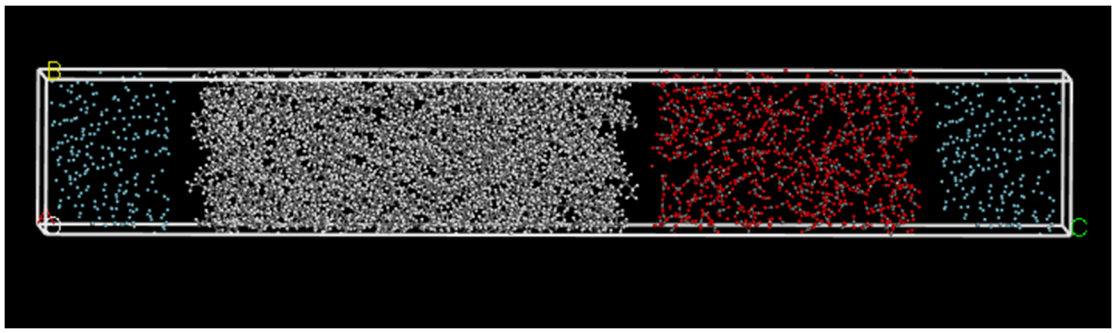

Figure 16. Initial Configurations for Molecular Simulation

The script written in the flooding module of MS software is shown in the figure. The corresponding temperature settings are 313K, 333K, and 353K, the pressure settings are 10MPa, 15MPa, and 20MPa, and the time step is 15,000.

2.3.2. Simulation Results and Analysis

CO_2 Flooding Simulation in Quartz Pores (Taking 313 K and 20 MPa as an Example):

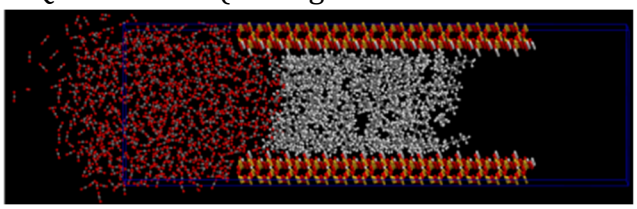

Figure 17. Simulation Results of CO_2 Flooding in Quartz Pores

ISSN: 2688-8645

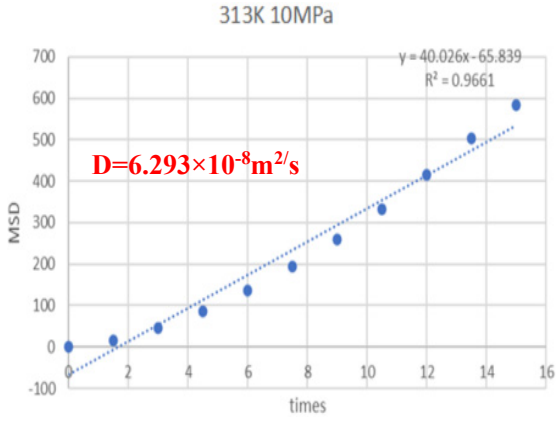

Figure 18. Relationship Curve Between Mean Square Displacement (MSD) and Simulation Time in the Model

Table 5. Diffusion Coefficients of CO_2 Flooding in Pores at Different Scales

Microscale	T/K	P/MPa	Diffusion Coefficient/ ($\times10^{-8}m^2/s$)	Macroscale	T/K	P/MPa	Diffusion Coefficient/ ($\times10^{-8}m^2/s$)
Molecular Simulation	313	10	6.293	(NMR) Experiment	313	10	1.193
		15	6.592			15	1.372
		20	6.653			20	1.453
	333	10	7.213		333	10	2.003
		15	7.753			15	2.262
		20	8.187			20	2.403
	353	10	7.626		353	10	2.203
		15	8.466			15	2.472
		20	8.737			20	2.603

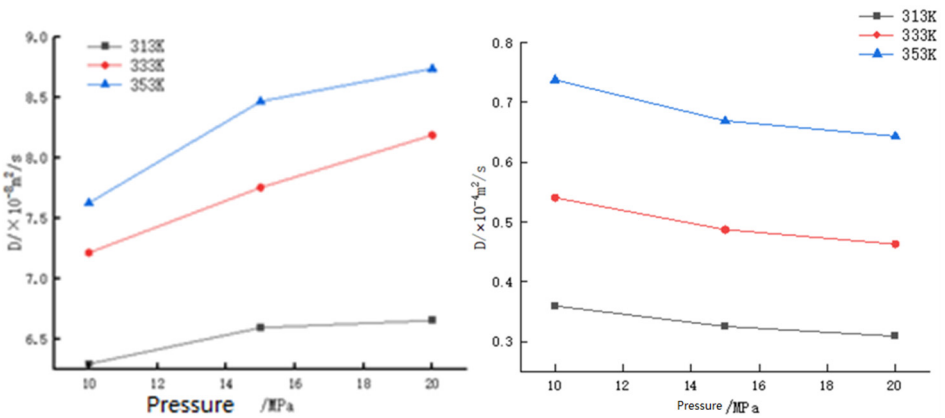

(a) Simulated Pore (b) Crude Oil Box

Figure 19. Diffusion Coefficients of CO_2 Flooding in Pores at Different Scales

3. Conclusion

The difference in pore structures hinders diffusion in porous media, with diffusion coefficients following the order: pure crude oil box > simulated pores > experimental pores. Near the miscibility pressure, the increase in CO_2 flooding diffusion coefficient is most significant, which rises with increasing temperature and pressure: an increase of $1.112\times10^{-8}m^2/s$ per MPa pressure increment and $1.874\times10^{-8}m^2/s$ per Kelvin temperature increment.

As indicated by the diffusion coefficient table of the CO_2-porous media system: The diffusion coefficient gradually increases with the increase in initial pressure. Different from diffusion in pure fluids, during the diffusion process in porous media, the effect of pressure changes on molecular kinetic energy outweighs that on fluid viscosity and density changes. At the miscibility pressure, the increase in CO_2 diffusion coefficient is particularly significant.

References

[1] SHENG J J. Critical review of field EOR projects in shale and tight reservoirs[J]. Journal of Petroleum Science and Engineering,2017,159:654-665.

[2] ZBOROWSKI M. How Conoco Phillips solved its big data problem[J]. Journal of Petroleum Technology, 2018, 70(7): 21-26.

[3] GOMAA A M, NINO-PENALOZA A, MCCARTNEY E, et al. Engineering solid particulate diverter to control fracture complexity: Experimental study[R]. SPE179144, 2016.

[4] Yu W, Lashgari H, Sepehrnoori K. Simulation study of CO2 huff-n-puff process in Bakken tight oil reservoirs[C]. SPE 169575, 2014.

[5] Bai J, Liu H, Wang J, et al. CO2, water and N2 injection for enhanced oil recovery with spatialarrangement of fractures in tight-oil reservoirs using huff-n-puff[J]. Energies, 2019, 12(5): 823.

[6] Wang Q, Jiang R, Cui Y, et al. Pre-Darcy flow behavior of CO2 Huff-n-Puff development in Fuyu tight formation: Experiment and numerical evaluation[J]. Journal of Petroleum Science and Engineering, 2020, 186: 106773.

[7] Du D, Li C, Song X, et al. Experimental study on residue oil distribution after the supercritical CO2 huff-n-puff process in low permeability cores with Nuclear Magnetic Resonance (NMR)[J]. Arabian Journal of Chemistry, 2021, 14(10): 103355.

[8] Zhang H, Wang S, Yin X, et al. Soaking in CO2 huff-n-puff: A single-nanopore scale study[J]. Fuel, 2022, 308:122026.

[9] HUANG Liang, ZHOU Wen, XU Hao, et al. Dynamic flfluid states in organic-inorganic nanocomposite: Implications for shale gas recovery and CO2 sequestration[J]. Chemical Engineering Journal, 2021, 411: 128423.

[10] Pang, Y.. , Soliman, M. Y., Deng, H.. , and Hossein Emadi. Effect of Methane Adsorption on Stress-Dependent Porosity and Permeability in Shale Gas Reservoirs. [C] Paper presented at the SPE Low Perm Symposium, Denver, Colorado, USA, May 2016.

[11] Mingyao Wei, Jishan Liu, Xiating Feng, Chunguang Wang, Fubao Zhou, Evolution of shale apparent permeability from stress-controlled to displacement-controlled conditions, [J] Journal of Natural Gas Science and Engineering, Volume 34, 2016, Pages 1453-1460, ISSN 1875-5100.

[12] Xue-wu W, Pufu X, Zheng-ming Y, et al. Laboratory and field-scale parameter optimization of CO2 huff–n–puff with the staged-fracturing horizontal well in tight oil reservoirs[J]. Journal of Petroleum Science and Engineering,2020,186:106703.

[13] Shovkun I, Espinoza DN. Coupled fluid flow-geomechanics simulation in stress-sensitive coal and shale reservoirs: impact of desorption-induced stresses, shearfailure, and fines migration. [J]Fuel 2017;195:260–72.

[14] JILL T, NICK F, MARC S, et al. Tank development in the Midland Basin, Texas: A case study of super-charging a reservoir to optimize production and increase horizontal well densities[R]. URTeC2902895-MS, 2018.

[15] KELVIN A, JOHN Y, DEREK E, et al. Laboratory evaluation of multiphase permeability evolution in tight sandstones: Impact of slickwater and friction reducers[R]. SPE 180250-MS,2016.